REVISION January 19th 2018

$CaSiO_3$-perovskite in diamond confirms the recycling of oceanic crust into the lower mantle

F. Nestola[1], N. Korolev[2, 3], M. Kopylova[2], N. Rotiroti[4], D.G. Pearson[5], M.G. Pamato[6], M. Alvaro[7], L. Peruzzo[8], J.J. Gurney[9], A.E. Moore[10], J. Davidson[11]

1: Dipartimento di Geoscienze, Università degli Studi di Padova, Via G. Gradenigo 6, I-35131, Padova, Italy
2: Department of Earth, Ocean and Atmospheric Sciences, University of British Columbia, V6T 1Z4 Vancouver, Canada
3: Institute of Precambrian Geology and Geochronology RAS, 199034, St. Petersburg, Russia
4: Dipartimento di Scienze della Terra, Università degli Studi di Milano, Via Botticelli 23, I-20133 Milano, Italy
5: Department of Earth and Atmospheric Sciences, University of Alberta, Edmonton, Canada T6G 2E9
6: Department of Earth Sciences, University College London, Gower St, London WC1E 6BT, UK
7: Department of Earth and Environmental Sciences, University of Pavia, Via Ferrata 1, I-27100 Pavia, Italy
8: CNR-Istituto di Geoscienze e Georisorse – Sezione di Padova, Via G. Gradenigo 6, I-35131, Padova, Italy
9: University of Cape Town, Cape Town, South Africa, john.gurney@msgroup.net
10: Rhodes University, Grahamstown, South Africa, andy.moore.bots@googlemail.com
11: Petra Diamonds, Bryanston, South Africa, jim@petradiamonds.com

Laboratory experiments and seismology have created a clear picture of the major minerals expected to comprise the deeper parts of Earth's mantle. Finds of some of these phases in super-deep diamonds have confirmed part of this picture [1-5]. A striking exception is the high-pressure perovskite structured polymorph of $CaSiO_3$. This mineral – inferred to be the fourth most abundant in Earth - has never been found in nature. As the major host for Ca and heat-producing elements K, U and Th in the transition zone and lower mantle, it is critical to establish its presence. Here we document the first discovery of the perovskite-structured polymorph of $CaSiO_3$ in nature, included within a diamond from the Cullinan kimberlite, South Africa. The mineral is intergrown with ~ 6% $CaTiO_3$. The Ti-rich nature of this association indicates a bulk composition consistent with derivation from basaltic oceanic crust subducted to pressures equivalent to depths of the uppermost lower mantle. The relatively heavy carbon isotopic composition of the surrounding diamond, $\delta^{13}C = -2.3 \pm 0.5‰$, together with the pristine high-pressure $CaSiO_3$ structure, provides evidence of the recycling of oceanic crust and surficial carbon to lower mantle depths.

A key goal of solid Earth geosciences is to establish the mineralogy of Earth's mantle throughout its depth as it acts a primary control on mantle dynamics and chemistry. Diamonds are unique windows in this regard, providing access to the deepest intact material from Earth's interior through included minerals. Over three decades, a growing number of studies have used a class of diamonds known as "super-deep" diamonds to study mantle processes in the deep sublithospheric mantle, the transition zone and the lower mantle[1-6]. Pioneering studies[1-3] suggested that some of the

assemblages included within super-deep diamonds represented samples of the lower mantle and transition zone, variably retrogressed to lower pressures. Later studies cautioned that some of these assemblages and minerals might originate at shallower depths[7,8], though still beneath the lithosphere.

The most common minerals found within super-deep diamonds are ferropericlase [(Mg,Fe)O] and $CaSiO_3$[1-3,9]. Ferropericlase is stable at most pressure and temperature conditions in the mantle and hence, when found as a single inclusion within diamond, this mineral cannot be considered an unambiguous indicator of a super-deep origin[7].

The $CaSiO_3$ phase found within super-deep diamonds typically has the crystal structure of walstromite ($BaCa_2Si_3O_9$)[1,6,8,9]. Perovskite-structured $CaSiO_3$ (Ca-Pv) is considered one of the most important components in the Earth's lower mantle, comprising approximately 7% of a peridotitic mantle composition and ~23% of the volume of a subducted mid-ocean ridge basalt slab[9-11]. As such, it is likely to be the fourth most abundant terrestrial mineral. Within a peridotitic lower mantle, Ca-Pv is the dominant sink for Ca and for incompatible elements, including the key heat-producing elements K, U and Th[12]. However, Ca-Pv has so far never been found in nature and even high-pressure laboratory experiments have failed to quench it as a metastable phase at the Earth's surface. While initial studies of super-deep diamonds made a clear case for the presence of Ca-Pv[1-4], their structure was either undetermined or documented to be the lower-pressure polymorph - $CaSiO_3$-walstromite - and interpreted as a back-transformation of perovskite-structured $CaSiO_3$. The $CaSiO_3$-perovskite to $CaSiO_3$-walstromite phase transformation would require a volume change[13] of about 28% that is impossible for diamond to accommodate due to its extremely high bulk modulus[14]. The absence of healed fractures in the diamond host studied by [13] implies that $CaSiO_3$-walstromite, in that case, is unlikely to represent inverted $CaSiO_3$-perovskite. Plastic deformation of the diamond lattice could accommodate some of the volume change necessary for

68 the inclusion's phase transformation. Although plastic deformation is well documented in super-
69 deep diamonds[15], it has never been quantified and the amount of deformation would have to be
70 substantial. Thus, though some super-deep diamonds with documented phase assemblages that
71 include ferropericlase, enstatite (inverted bridgmanite) and/or $CaSiO_3$-walstromite are likely to have
72 originated from lower mantle depths[1-4,9], there remains some ambiguity hence finding an un-
73 retrogressed silicate perovskite would provide very powerful confirmation of lower mantle
74 sampling by some super-deep diamonds.
75
76 Here we investigated an inclusion within a diamond from the Cullinan Mine, Gauteng Province,
77 Republic of South Africa. The Cullinan kimberlite is Group I in character, i.e., its chemistry and Sr-
78 Nd-Hf isotope signatures are thought to reflect a melt source from beneath the lithospheric mantle,
79 within the Earth's convecting mantle[16]. Cullinan mine is renowned for producing exceptionally
80 large diamonds such as the Cullinan diamond[6,17], most of which have been suggested to be super-
81 deep diamonds[6].
82
83 The $31\times26\times10$ μm^3 $CaSiO_3$ inclusion in diamond, exposed by polishing, was revealed by X-ray
84 diffraction, Raman spectroscopy and electron backscatter diffraction to have a perovskite structure.
85 To our knowledge, this represents the first finding of a non-reverted silicate perovskite-structured
86 $CaSiO_3$ phase found in nature and the first, including those synthesized in the laboratory, to be
87 preserved with its high-pressure structure at the surface of the Earth.
88
89 Cathodoluminescence imaging of the host diamond surrounding the Ca-Pv inclusion (Fig. 1) reveals
90 multiple growth zones and a complex internal structure, typical of super-deep diamonds[4,18]. FTIR
91 spectroscopy (Extended Data Figure 1) of the diamond host indicates a nitrogen content of 34 ppm,
92 with 97% in the B-aggregated form, i.e., the diamond host is type IaB. The low nitrogen content and
93 very high level of B aggregation are typical characteristics of other super-deep diamonds[4,19]

indicating prolonged residence at the high temperatures expected at transition zone and lower mantle depths.

The chemical composition of the CaPv inclusion, determined by electron microprobe, yields a nearly pure $CaSiO_3$ composition ($Ca_{0.98}Si_{0.98}O_3$), with minor impurities of Ti, Al, Fe, Mg totaling 0.04 atoms per formula unit (Extended Data, Table 1).

Backscatter electron imaging and EDS element maps (Fig. 2) show that the Ca-Pv crystal includes 14 irregular areas of $CaTiO_3$-perovskite between 1 and 7-8 μm with a stoichiometry of ~ $Ca(Ti_{0.92}Si_{0.07}Al_{0.02})O_3$. The size and abundance of the $CaTiO_3$ intergrowths within this Ca-Pv is very similar to the texture and abundance of inclusions reported in $CaSiO_3$-walstromite phases reported from Juina super-deep diamonds[20]. The 2D exposed surface of our Ca-Pv inclusion makes accurate estimation of its bulk composition difficult, but image analysis indicates that the host crystal, in bulk may have up to 6% by volume $CaTiO_3$. $CaTiO_3$-perovskite is a common mineral in nature and is stable well into the lower mantle[21]. In contrast, CaPv retaining its perovskite structure has no experimentally synthesised analogues at room temperature and pressure, unless significant $CaTiO_3$ is dissolved within its structure (~34 mol %[21]), far more than the $CaTiO_3$ component observed here. However, our discovery of natural CaPv, trapped in a diamond, with < 2 mol % $CaTiO_3$ component in the $CaSiO_3$-rich portion of the inclusion, indicates that unlike experiments, there must be natural P-T-t pathways that are capable of the metastable preservation of this phase.

X-ray diffraction data show the $CaSiO_3$ inclusion to have the perovskite structure. The small size of the inclusion (thickness estimated by confocal Raman spectroscopy to be ≤ 10 μm) and its entrapment within the diamond host resulted in only a limited number of measured diffraction reflections (n=91), of which only 9 were unique (Extended Data Table 2). The full 91 reflections were used to refine the Ca-Pv unit-cell parameters to yield:

120 $a = 5.397(4)$ Å, $b = 5.404(4)$ Å, $c = 7.646(4)$ Å, $Volume = 223.0(3)$ Å^3.

121 However, alternative unit-cell refinements using other numerical approaches could provide
122 significantly different unit-cell parameters that may differ by greater than 1%, due to the relatively
123 poor accuracy and precision of the *d*-spacings measured here. These larger than normal
124 uncertainties are typical when studying minerals of this size and arise not just from the limited
125 number of reflections but also due to the measurements being performed using an area detector,
126 which provides lower precision in *d*-spacing determination than a point detector. Such relatively
127 large uncertainty on the cell parameters makes any comparison with the unit cell volume of $CaTiO_3$
128 –perovskite unreliable, even though we can define the two structures as being very similar. Ewald
129 projections along the three crystallographic axes (Fig. 3a) indicate an orthorhombic unit-cell. The
130 unit-cell together with the chemical composition define the mineral to be perovskite-structured
131 $CaSiO_3$. Recent numerical simulations on "host-inclusion" systems[22], indicate that an inclusion
132 partly exposed to atmospheric pressure only loses a portion of its residual pressure, as a function of
133 the elastic properties of both the host mineral and the inclusion. The Ca-Pv inclusion studied here is
134 partly exposed at the diamond surface but with 2/3 of its volume still buried in the diamond host.
135 Thus, any measurements on this grain would be affected by some residual "pressure" still acting on
136 the inclusion, which in turn affects the X-ray diffraction data and Raman spectra.
137
138 Raman spectra (Fig. 3b) for the inclusion show that the $CaTiO_3$ perovskite spectrum is in excellent
139 agreement with $CaTiO_3$-perovskite Raman data from the RRUFF database[23] (Extended Data Fig. 2).
140 The $CaSiO_3$ and $CaTiO_3$ spectra are similar. Small differences are evident due to the presence of
141 two Raman peaks for the $CaSiO_3$ spectrum, which could belong to the lower-pressure $CaSiO_3$
142 polymorph wollastonite-2M[23]. This wollastonite polymorph is not stable at pressures higher than 3
143 GPa along a mantle geotherm [24], well below the diamond stability field. Hence its presence seems
144 likely due to minor partial inversion of the Ca-Pv phase owing to the polishing of the sample to
145 expose the inclusion, as reported in previous work[25].

The EBSD measurements collected on several areas of the grain provide no evidence that amorphous portions are present and confirm that the $CaSiO_3$ zones have perovskite-structure (Fig. 4). A typical EBSD pattern collected on the $CaSiO_3$ area (red circle), shown as the relative non-indexed EBSD pattern (Fig. 4) is complex and could not be indexed by a single phase. Indexing the pattern by using a combination of reference EBSD patterns for $CaTiO_3$-perovskite (Fig. 4c) and wollastonite-2M (Fig. 4d), accounts for the observed pattern, confirming the conclusions from X-ray and Raman work, that $CaSiO_3$ is present in this diamond with a perovskite-type structure.

We suggest that the natural Ca-Pv found trapped within our super-deep diamond originated as a result of unmixing, of the high-pressure solid solution $Ca(Ti,Si)O_3$. If the two phases exsolved from a homogenous bulk composition, this phase would contain ~ 3.9% TiO_2.

Our estimate of the stoichiometry of the original phase composition is:

$$(Ca_{0.98}Mg_{0.01}Fe_{0.01})(Si_{0.93}Ti_{0.06}Al_{0.01})O_3$$

This composition is consistent with those of $CaSiO_3$ crystallised in experiments from a MORB-like bulk composition at ~ 24 GPa[26] and is similar to the $CaSiO_3$ - walstromite/$CaTiO_3$ intergrowths found within Juina super-deep diamonds that were proposed to represent basalt-like compositions subducted to lower mantle depths and later retrogressed during ascent to Earth's surface[20]. The preservation of the high-pressure perovskite structure in the case of the Cullinan inclusion proves the derivation of such compositions from lower mantle depths.

The indicated subducted basaltic protolith of the Cullinan Ca-Pv inclusion suggests that we might expect to observe some evidence of a crustal parentage in the C isotopic composition of the host diamond. Its carbon isotopic composition is variable (Fig. 1; Extended Data: Table 3) with $\delta^{13}C$ values ranging from -2.3‰ to -4.6‰. The core region of the diamond, defined by CL-imaging (Fig. 1), contains the Ca-Pv inclusion and an average $\delta^{13}C$ value of -2.3 ±0.5‰, significantly lower than

the typical upper mantle value of -5.5‰[27]. In contrast, the outer rim region of the diamond has a composition (Mean $\delta^{13}C$ -4.1 ± 0.5‰) that is closer to the normal mantle value. Crustal carbon reservoirs have C isotopic compositions that are both heavier and lighter than the typical upper mantle value. While isotopically lighter carbon (below -25‰) has been found in super-deep diamonds from Juina, proposed to be derived from subducted basalt protoliths[20,28], heavier carbon isotopic compositions, such as those measured in the core of our Cullinan diamond, have also been reported in super-deep diamonds from both Sao Luis/Juina (Brazil) and from Kankan (Guinea)[18-20]. If the $\delta^{13}C$ value of -2.3‰ is compared with the median value (-4.91 ‰) of 1473 published analyses of lithospheric diamonds containing peridotitic inclusions – a group of diamonds usually accepted to have minimal subducted influence[27] - it can be defined as an outlier, beyond 3 times the median absolute deviation. Such anomalously heavy C isotopic compositions are thought to reflect a greater influence of subducted carbonate in the fluid that formed these super-deep diamonds[18,19]. The C isotope compositions of the rim of the Cullinan diamond (Fig. 1) may represent an overgrowth that grew under upper mantle conditions, or from a distinct source of carbon in the lower mantle. Regardless, the isotopically heavy $\delta^{13}C$ values of the portion of the diamond containing the Ca-Pv inclusion lends support to its origin from a subducted basaltic protolith.

Our discovery of perovskite-structured $CaSiO_3$ in a super-deep diamond firmly establishes this phase as a component in Earth's deep mantle, confirming previous suggestions that lower pressure $CaSiO_3$ polymorphs included in these diamonds may represent retrogressed Ca-Pv[1-4,9]. The estimated original bulk composition of the Cullinan Ca-Pv inclusion is consistent with compositions stable in subducted oceanic basalt protoliths at ~ 24 GPa, in the uppermost lower mantle[26]. Our finding thus confirms the expectation from calculation[10] and high-pressure experiments[21,25,] that Ca-Pv is the chief Ca-bearing phase in the lower mantle in both basic and ultrabasic compositions, reaching up to 23 vol% in MORB-like compositions[26]. The combined bulk composition of the Ca-Pv phase found here provides overwhelming evidence of the return of recycled oceanic crust into

Earth's lower mantle[20] while the relatively heavy C isotopic composition of the diamond in contact with the inclusion indicates the subduction of crustal carbon to lower mantle depths.

AKNOWLEDGEMENTS

Nature thanks Dr. Ben Harte and another anonymous reviewer for their contribution to the peer review of this work. Margo Regier is thanked for proof-reading. FN is supported by the ERC Starting Grant n. 307322. MK work and sample collection was possible due to an NSERC Discovery grant. NK acknowledges funding from the Dr. Eduard Gübelin Association through a 2015 Dr. Eduard Gübelin research scholarship. DGP was funded by an NSERC CERC award. MA was supported by the European Research Council (ERC) under the European Union's Horizon 2020 research and innovation program (grant agreement 714936) "TRUE DEPTHS" and by the SIR-MIUR grant (RBSI140351) "MILE DEEp". Dr. Lucio Litti and Prof. Moreno Meneghetti of the Laboratory of Nanostructures and Optics of Department of Chemical Sciences, University of Padova, are thanked for their crucial help in acquiring and interpreting the Raman data.

AUTHOR CONTRIBUTIONS

FN conceived the study, wrote the initial manuscript and performed X-ray diffraction and micro-Raman measurements. NK found the mineral, made original mineral identifications on a confocal Raman spectrometer (EOAS, UBC), performed microprobe and CL measurements, prepared samples for SIMS measurements and assisted with the manuscript preparation. MK supervised the study of the Cullinan diamond collection acquired through JG, AEM and JD and assisted with manuscript preparation. DGP made the geochemical interpretations and led the manuscript revisions. MGP assisted with the manuscript preparation and crystallographic interpretations. NR, MGP and MA assisted with the X-ray data interpretation. LP collected and interpreted the EBSD data. JG, AEM and JD designed the sampling program.

COMPETING INTERESTS

The authors declare no competing financial interests.

REFERENCES

1. Joswig, W., Stachel, T., Harris, J.W., Baur, W., Brey, G.P. New Ca-silicate inclusions in diamonds – tracers fromn the lower mantle. Earth & Planetary Science Letters. **173**, 1-6 (1999).
2. Harte, B., Harris, J.W., Hutchison, M.T., Watt, G.R. & Wilding, M.C. Lower mantle mineral associations in diamonds from Sao Luiz, Brazil. In: Fei, Y., Bertka, C.M. Mysen, B.O. (eds) Mantle petrology: field observations and high pressure experimentation; A tribute to Francis R. (Joe) Boyd. *Geochemical Society Special Publication* **No 6**, pp 125-153 (1999).
3. Stachel, T., Harris, J. W., Brey, G. P. & Joswig, W. Kankan diamonds (Guinea) II: lower mantle inclusion paragenesis. *Contrib. to Mineral. Petrol.* **140,** 16–27 (2000).
4. Hayman, P. C., Kopylova, M. G. & Kaminsky, F. V. Lower mantle diamonds from Rio Soriso (Juina area, Mato Grosso, Brazil). *Contrib. to Mineral. Petrol.* **149,** 430–445 (2005).
5. Pearson, D. G. *et al.* Hydrous mantle transition zone indicated by ringwoodite included

within diamond. *Nature* **507,** 221–224 (2014).
6. Smith, E. M. *et al.* Large gem diamonds from metallic liquid in Earth's deep mantle. *Science* **354,** 1403–1405 (2016).
7. Brey, G. P., Bulatov, V., Girnis, A., Harris, J. W. & Stachel, T. Ferropericlase - a lower mantle phase in the upper mantle. *Lithos* **77,** 655–663 (2004).
8. Thomson, A., Walter, M.J., Kohn, S.C., Brooker, R.A. Slab melting as a barrier to deep carbon subduction. *Nature* **529**, 76-79 (2016).
9. Harte, B. & Hudson, N.F.C. Mineral associations in diamonds from the lowermost upper mantle and uppermost lower mantle. In: D.G. Pearson et al. (eds) *Proceedings of the 10th International Kimberlite Conference, vol. 1, Special issue of the Geological Society of India*, pp 235-253 (2013).
10. Stixrude, L & Lithgow-Bertelloni, C. Geophysics of chemical heterogeneity in the mantle. *Ann. Rev. Earth Planet. Sci.* **40**, 569-595 (2012).
11. Ringwood, A. E. *Composition and Petrology of the Earth's Mantle*. McGraw-Hill, New York (1975).
12. Corgne, A. & Wood, B. J. Trace element partitioning and substitution mechanisms in calcium perovskites. *Contrib. to Mineral. Petrol.* **149,** 85–97 (2005).
13. Anzolini, C. *et al.* Depth of formation of $CaSiO_3$-walstromite included in super-deep diamonds. *Lithos* **265,** 138–147 (2016).
14. Angel, R. J., Alvaro, M., Nestola, F. & Mazzucchelli, M. L. Diamond thermoelastic properties and implications for determining the pressure of formation of diamond-inclusion systems. *Russ. Geol. Geophys.* **56,** 211–220 (2015).
15. Cayzer, N. J., Odake, S., Harte, B. & Kagi, H. Plastic deformation of lower mantle diamonds by inclusion phase transformations. *Eur. J. Mineral.* **20,** 333–339 (2008).
16. Nowell, G. M., Pearson, D. G., Bell, D.R., Carlson, R.W., Smith, C. B., Kempton, P.D. and Noble, S.R. Hf isotope systematics of kimberlites and their megacrysts: New constraints on their source region. *J. Petrology*, **45**, 1583-1612 (2004).
17. Moore, AD. The origin of large irregular gem-quality type II diamonds and the rarity of blue type IIb varieties. South African Journal of Geology **117**, 219-236 (2014).
18. Palot, M., Pearson, D. G., Stern, R. A., Stachel, T. & Harris, J. W. Isotopic constraints on the nature and circulation of deep mantle C-H-O-N fluids: Carbon and nitrogen systematics within ultra-deep diamonds from Kankan (Guinea). *Geochim. Cosmochim. Ac.* **139,** 26–46 (2014).
19. Stachel, T., Harris, J. W., Aulbach, S. & Deines, P. Kankan diamonds (Guinea) III: δ13C and nitrogen characteristics of deep diamonds. *Contrib. to Mineral. Petrol.* **142,** 465–475 (2002).
20. Walter, M. J. *et al.* Deep Mantle Cycling of Oceanic Crust: Evidence from Diamonds and Their Mineral Inclusions. *Science* **334,** 54–57 (2011).
21. Kubo, A., Suzuki, T. & Akaogi, M. High pressure phase equilibria in the system $CaTiO_3$-$CaSiO_3$: stability of perovskite solid solutions. *Phys. Chem. Miner.* **24**, 488-494 (1997).
22. Mazzucchelli, M.L., Burnley, P., Angel, R.J., Morganti, S., Domeneghetti, M.C., Nestola, F. & Alvaro, M. Elastic geothermobarometry: corrections for the geometry of the host-inclusion system. Geology, in press, doi: 10.1130/G39807.1.
23. Lafuente, B., Downs, R.T., Yang, H. & Stone, N. in Highlights in Mineralogical Crystallography 1–29 (2016).
24. Gasparik, T., Wolf, L. & Smith, C.M. Experimental determination of phase relations in the $CaSiO_3$ system from 8 to 15 GPa. *Am. Mineral.* **79**, 1219-1222 (1994).
25. Ringwood, A.E. & Major, A. Synthesis of majorite and other high pressure garnets and perovskites. *Earth Planet. Sci. Lett.* **12**, 411-418 (1971).
26. Hirose, K. & Fei, Y. Subsolidus and melting phase relations of basaltic composition in the uppermost lower mantle. *Geochim. Cosmochim. Acta.* **66**, 2099-2108 (2002).
27. Cartigny, P., Palot, M., Thomassot, E. & Harris, J. W. Diamond Formation: A Stable Isotope

Perspective. *Annu. Rev. Earth Planet. Sci.* **42,** 699–732 (2014).
28. Burnham, A.D. *et al.* Stable isotope evidence for crustal recycling as recorded by superdeep diamonds. *Earth Planet. Sci. Lett.* **432,** 374–380 (2015).

Figure captions

Figure 1. Cathodoluminescence image and carbon isotopic composition of the diamond containing the $CaSiO_3$ (Ca-Pv) inclusion. Inclusion of Ca-Pv shown in yellow. Spots at five different locations give carbon isotopic compositions of the diamond host, in $\delta^{13}C$ notation, where

$\delta^{13}C = [(^{13}C/^{12}C)_{sample}/(^{13}C/^{12}C)_{PDB} -1]x1000$ in which PDB is the Pee Dee Belemenite reference material.

Figure 2. Back-scattered electron image of the CaPv inclusion still included in host diamond and energy-dispersive X-ray spectroscopy elemental maps. Back-scattered electron image (a) of CaPv inclusion (dark-grey) surrounded by the diamond host (black) showing inclusions of $CaTiO_3$ perovskite (light gray). Images b, c and d are energy-dispersive X-ray spectroscopy elemental maps of Ca, Ti and Si, respectively, with intensity of colour (black within grain outline though to saturation in specific colour) proportional to element concentration.

Figure 3. Ewald projections of X-ray diffraction data and Raman spectroscopic results. The Ewald projections (a) were made along three different orientations for $CaSiO_3$-perovskite. The projections were obtained using Crysalis software (Rigaku-Oxford Diffraction). Baseline corrected Raman spectra in (b) compare spectra from the CaPv inclusion with that of $CaTiO_3$ - perovskite found as an intergrowth (Fig. 2a). Raman spot size was ~1.1 μm, spectral resolution 3 cm^{-1}.

Figure 4. Electron backscatter diffraction (EBSD) images of the Ca-Pv inclusion in diamond. EBSD image collected on the red circle (a) relative to the $CaSiO_3$ area of our inclusion. In (b) the non-indexed EBSD pattern is shown, whereas in (c) and (d) the pattern was indexed with the $CaTiO_3$ and wollastonite-2M reference patterns.

On-line Methods

Micro-Raman spectroscopy

The $CaSiO_3$-perovskite sample was analysed by a InVia Renishaw micro-Raman spectrometer installed at the Department of Chemical Sciences, University of Padova. Spectra were baseline corrected. A 632.8 nm excitation laser was used at a power of 7 mW. The Raman spectrum of the $CaSiO_3$-perovskite crystal was collected for 40 seconds using a 50× objective with a spatial resolution of 1.1 μm and a spectral resolution estimated to be ~ 3 cm^{-1}. The most intense Raman peaks observed for the $CaSiO_3$-perovskite inclusion are, in order of decreasing intensity (in cm^{-1}): 774, 247, 470, 337, 181 and 226.

A direct comparison between the Raman spectrum of natural $CaSiO_3$-perovskite with that of $CaTiO_3$ inclusions and those reported by the RRUFF Raman database[23] indicate that the two spectra are very similar. A small but important difference is due to the presence of limited traces of wollastonite 2M on the natural $CaSiO_3$-perovskite Raman spectrum (see peaks at 971 and 637 cm^{-1}), which, as expected, are not evident for $CaTiO_3$ perovskite inclusions.

In terms of the Raman peak assignment, it must be noted that based on the results of [29], the broad Raman bands in the 650-850 cm^{-1} region are due to second order Raman scattering and that only the sharp peaks in the 200-500 cm^{-1} region are first-order Raman bands. For our purpose, however, the entire Raman spectrum of natural $CaSiO_3$-perovskite is considered, regardless of the first or second order scattering, for a direct comparison mainly with $CaTiO_3$ perovskite and wollastonite.

The strong similarity in the Raman spectra between $CaTiO_3$ and $CaSiO_3$ perovskites in Fig. 3b could be used to invoke the possibility that the spectra are dominated by a larger underlying, unexposed portion of the $CaTiO_3$ phase and also permit the possibility that the $CaSiO_3$ regions of the inclusion are amorphous, as we would expect a general Raman shift for the $CaSiO_3$ bands toward higher wavenumbers. This possibility can be discounted for a number of reasons. Firstly, the partially exposed inclusion is under some stress and this will affect the Raman band shift depending on the elastic properties of the two perovskites. More importantly, the Raman spectra of such a large amorphous area of $CaSiO_3$ would be totally distinct from that measured here (Fig. 3b), and would be, in such a scenario, characterized by the presence of three very intense Raman bands at ~ 370, 640 and 970 cm^{-1} (depending on the P and T conditions[30,31]). These Raman bands are absent in the spectrum of the $CaSiO_3$ portion of the perovskite-structured inclusion in diamond. Also, the spot size and confocal nature of the Raman measurements made here are too small to be significantly influenced by the spatially associated $CaTiO_3$ intergrowth.

Cathodoluminescence

The cathodoluminescence SEM image (CL) shown in Figure 1 of the main text was obtained using a Philips XL 30 scanning electron microscope with a CL attachment consisting of a Hamamatsu R376 photomultiplier

tube (EOAS UBC, Vancouver, Canada). The accelerating voltage was 20 keV and the electron beam current was 100 μA.

Infrared spectroscopy

Infrared spectra were collected for the diamond hosting natural $CaSiO_3$-perovskite on a Nicolet 6700 Fourier transform infrared spectrometer (Vancouver, Canada). The absorbance spectra for a sample were measured at maximum light transmission. Background spectra were collected for 120 s prior to the analysis and were subtracted from each measured absorbance spectra. Count times for spectra were 40 seconds at a spectral resolution of 0.5 cm^{-1}. The nitrogen concentration and aggregation were determined by the procedure described in [32] using the spreadsheet ("FTIR analyser 3d") provided by John Chapman (Rio Tinto Diamonds Ltd.). Preliminary processing and baseline determination were made using EssentialFTIR® software. The analytical and processing error is ±10% (1 sigma, relative error). The FTIR spectrum of the diamond from Cullinan studied here is shown in Extended Data Fig. 1.

Electron Microprobe analysis

Quantitative chemical analyses were undertaken on a fully automated CAMECA SX-50 electron microprobe (University of British Columbia, Department of Earth, Ocean and Atmospheric Sciences), operating in the wavelength-dispersion mode with the following operating conditions: excitation voltage, 15 kV; beam current, 20 nA; peak count time, 20 s; background count-time, 10 s; actual spot diameter, 5 μm. Data reduction was done using the 'PAP' φ(ρZ) method[32]. Detection limits for most oxides were below 0.08 wt.%, detection limits for Cr_2O_3, MnO_2, and NiO were less than 0.12 wt.%. Due to the crystal size of natural $CaSiO_3$-perovskite and the presence of inclusions of $CaTiO_3$ perovskite, we were able to perform only three reliable analyses; the results are reported in EXTENDED DATA Table 1. Na and K were not analysed.

Scanning Electron Microscopy and Energy Dispersive X-ray Spectroscopy

Our newly discovered natural $CaSiO_3$-perovskite was studied by SEM-EDS in order to investigate the distribution of Ca, Si and Ti over the grain. We used a CamScan MX3000 electron microscope equipped with a LaB6 source, four-quadrant solid state back-scattered electron (BSE) detector and an EDAX EDS

system for micro-analysis installed at the Department of Geosciences, University of Padova. The analytical conditions were: accelerating voltage, 20 kV; filament emission, □13 nA; working distance, 27 mm. The BSE image and the relative EDS Ca-Si-Ti map are shown in Figure 2.

Single-crystal micro-X-ray diffraction

Single-crystal X-ray diffraction measurements were performed using a Rigaku-Oxford Diffraction Supernova goniometer installed at the Department of Geosciences, University of Padova, equipped with a Dectris Pilatus 200 K area detector and a Mova X-ray microsource (MoKα-radiation) operating at 50 kV and 0.8 mA. The sample to detector distance was 68 mm. Data reduction was performed using the CrysAlis software (Rigaku Oxford Diffraction). Diffraction data are reported in Extended Data Table 2 and are compared to those of a reference $CaTiO_3$ measured on a single crystal[34] having the following unit-cell parameters: a = 5.388(1) Å, b = 5.447(1) Å, c = 7.654(1) Å, V = 224.63(1) Å3.

Carbon isotope analyses

Carbon isotope compositions ($\delta^{13}C$), reported in EXTENDED DATA Table 3 were determined using a Cameca IMS 7f-GEO secondary ion mass spectrometer (Caltech, USA). The polished diamond investigated was pressed into an indium mount with a 1" diameter aluminium holder. Natural reference diamonds with reference values of $\delta^{13}C$ between -13.6‰ (2σ = 0.3) and -2.5-2.6‰ (2σ = 0.3) were used to determine the instrumental mass fractionation and drift before and after sample analyses. Diamonds were coated with gold (20 nm). Analyses were conducted using $133Cs^+$ at 10 keV impact energy and a beam current of ~4 nA. The 15 μm diameter $133Cs^+$ primary-ion beam was used for pre-sputtering. During analysis, the ion beam diameter was reduced to 5 μm. Secondary ions of 12C and 13C were extracted at -9 keV. No e-gun charge compensation was required. The secondary ion energy bandwidth was 90 eV. 13C-/12C- ratios were measured using dual Faraday cups (FC1 for 12C- and FC2 for 13C-). The mass resolving power ($R = M/\Delta M$) was 2900. The ^{12}C as well as ^{13}C ions were counted for 1 second, in each cycle (30 cycles in total). Total time spent on each spot was 8 minutes. The standard deviation of the analyses is estimated at about 0.4 to 0.5 ‰ at the two-sigma (95% uncertainty) level.

Electron Backscatter Diffraction

EBSD analyses were performed at CNR-ICMATE (Padova, Italy) using a Quanta 200F FEG-ESEM (FEI Company) operating in high vacuum mode at an accelerating voltage of 30 kV, emission 174 μA, spot 4.5, without any conductive coating. EBSD patterns were collected at 10 mm WD and 75° specimen tilt, using an EDAX Digiview EBSD system. The instrument is controlled by the OIMTM 5.31 software, which contains a large EBSD pattern database.

Statistical analysis of diamond carbon isotope composition

We used a compilation of 1473 C-isotope analyses of diamonds containing inclusions of lithospheric peridotite paragenesis, from the dataset used by Huber (1981) [35]. We calculated the median absolute deviation for this dataset using a bespoke Excel spread sheet, using formulae given in [36], using a *b* factor of 1.4826 and a very conservative threshold factor of 3 [36].

References – On-line Methods

29. McMillan, P. & Ross, N. The Raman spectra of several orthorhombic calcium oxide perovskites. Phys. Chem. Miner. **16**, 21–28 (1988).
30. Yin, C.D., Okuno, M., Morikawa, H., Marumo, F. & Yamanaka, T. Structural analysis of $CaSiO_3$ glass by X-Ray diffraction and Raman spectroscopy. *J. Non-Cryst. Solids* **80**, 167-174 (1986).
31. Zerr, A., Serghiou, G. & Boehler, R. Melting of $CaSiO_3$ perovskite to 430 kbar and first in-situmeasurements of lower mantle eutectic temperatures. *Geophys. Res. Lett.* **24**, 909-912 (1997).
32. Mendelssohn, M.J., Milledge, H.J. Geologically significant information from routine analysis of the Mid-Infrared spectra of diamonds. Int. Geol. Rev. **37**, 95-110 (1995)
33. Pouchou, J.L., Pichoir, F. "PAP" (φ ρZ) correction procedure for improved quantitative microanalysis. In: Armstrong JT (ed) Microbeam Analysis. San Francisco Press, San Francisco, pp 104-106 (1985).
34. Buttner, R.H., Maslen, E.N. Electron Difference Density and Structural Parameters in CaTiO3. Acta Crystallogr. C 48, 644-649 (1992).
35. Stachel, T., Harris, J.W. & Muehlenbachs, K. Sources of carbon in inclusion bearing diamonds. Lithos **112**, 625-637 (2009).
36. Huber, P. Robust Statistics. New York: Wiley (1981)

Data Availability Statement

All relevant data are included in the Extended Data section of this manuscript (Extended Data Tables 1-3, forming the basis of Figs 1-4, except original spectral data and electron microprobe data which are available from the first author.

Extended Data Table and Figure Legends

EXTENDED DATA Table 1. Chemical analyses for $CaSiO_3$-perovskite investigated in this work, including cation proportions (calculated on the basis of 3 oxygens) for the average value (Ave). The data were averaged for three spot analyses due to the extremely limited crystal size.

EXTENDED DATA Table 2. List of *d*-spacings with their relative intensities (I) with the most intense peak at 100 and hkl indexes for $CaSiO_3$-perovskite obtained by single-crystal X-ray micro diffraction compared with the *d*-spacings from a reference $CaTiO_3$ [34].

EXTENDED DATA Table 3. Carbon isotopic composition ($\delta^{13}C$, in ‰) and relative uncertainty for the host diamond enclosing the $CaSiO_3$-perovskite inclusions. The locations from 1 to 5 refer to positions annotated on Figure 1 of the main text.

EXTENDED DATA Figure 1. FTIR absorption spectrum, baseline corrected, of the diamond containing the $CaSiO_3$-perovskite inclusion.

EXTENDED DATA Figure 2. Comparison between the Raman spectra of $CaTiO_3$ studied in this work (blue) and $CaTiO_3$ reported in the RRUFF database[23] (card number R050456).

Footnote of the EXTENDED DATA Table 1
Cations calculated from data in column 2. Na and K were not analysed. Ave = Average. Stand. Dev. is the standard deviation of the 3 analyses used to construct the average in column 2. < D.L. denotes less than the detection limits listed in METHODS.

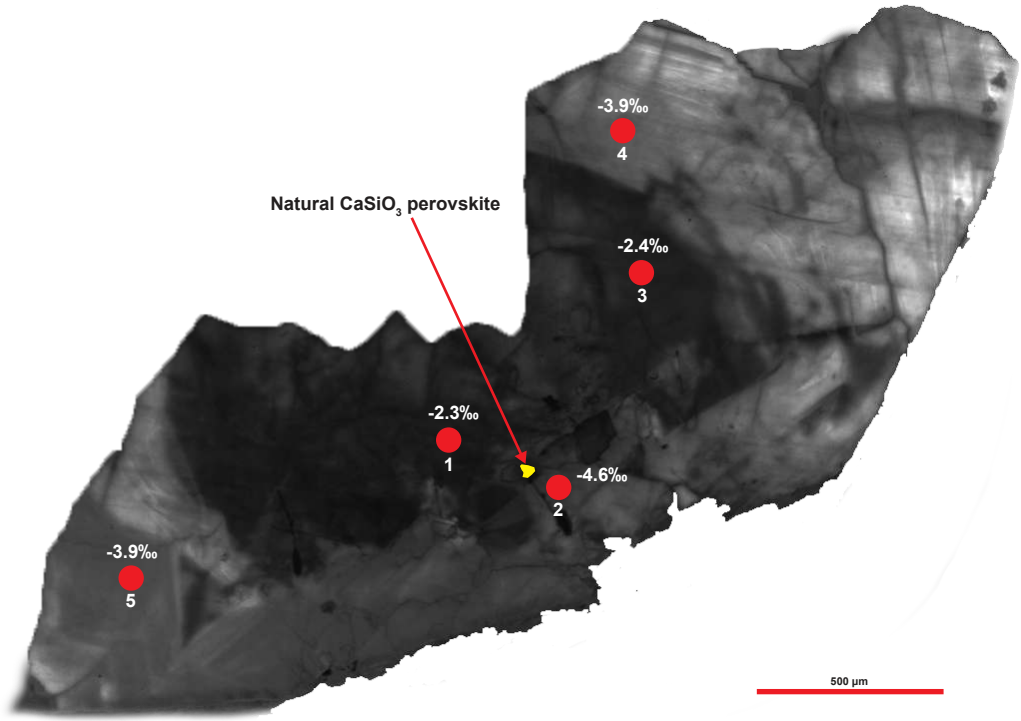
-3.9‰
4
Natural $CaSiO_3$ perovskite
-2.4‰
3
-2.3‰
1
-4.6‰
2
-3.9‰
5
500 µm

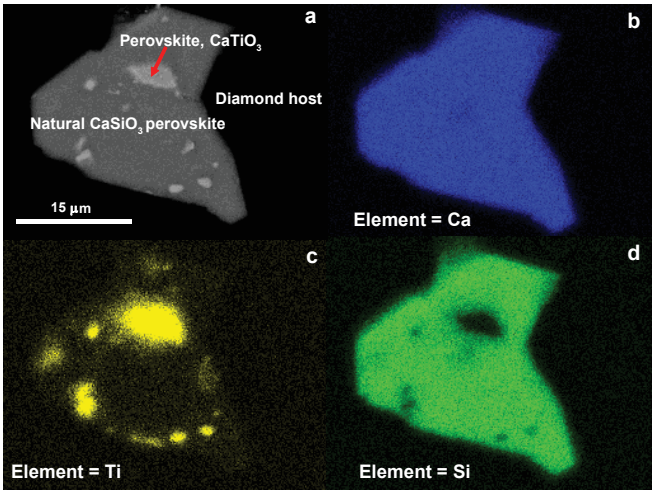
a
Perovskite, $CaTiO_3$
Diamond host
Natural $CaSiO_3$ perovskite
15 μm
b
Element = Ca
c
Element = Ti
d
Element = Si

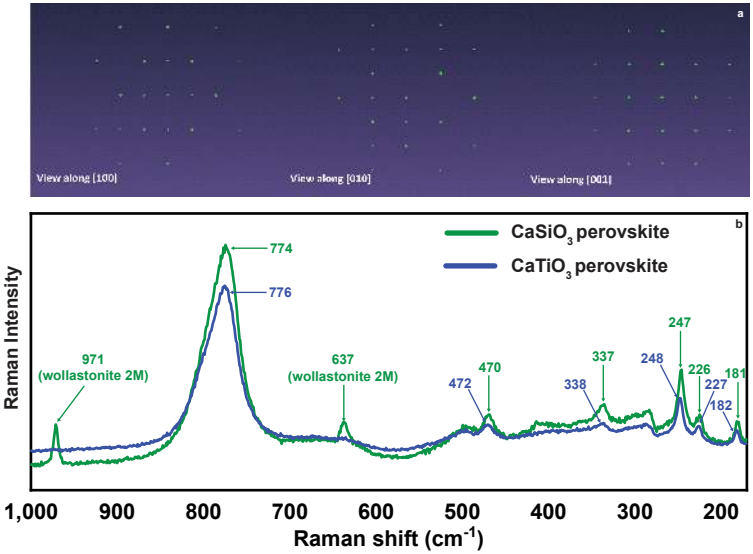
a
View along [100]
View along [010]
View along [001]
b
CaSiO3 perovskite
CaTiO3 perovskite
774
776
971
(wollastonite 2M)
637
(wollastonite 2M)
472
470
338
337
248
247
226
227
182
181
Raman Intensity
1,000
900
800
700
600
500
400
300
200
Raman shift (cm-1)

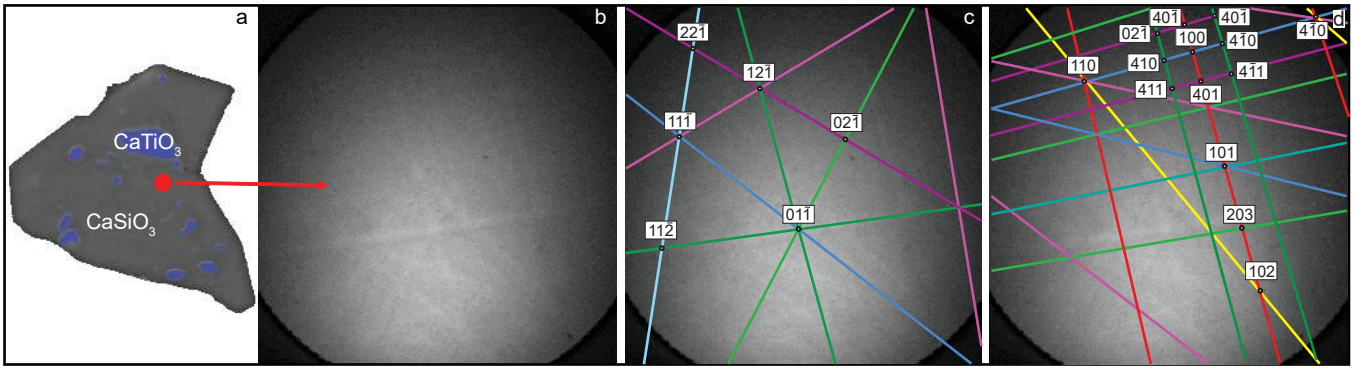
a
b
c
d
CaTiO3
CaSiO3
22$\bar{1}$
12$\bar{1}$
11$\bar{1}$
02$\bar{1}$
11$\bar{2}$
01$\bar{1}$
40$\bar{1}$
40$\bar{1}$
02$\bar{1}$
100
41$\bar{0}$
41$\bar{0}$
110
41$\bar{0}$
41$\bar{1}$
41$\bar{1}$
40$\bar{1}$
10$\bar{1}$
20$\bar{3}$
10$\bar{2}$